2024

# Biomass burning is a source of modern black carbon to equatorial Atlantic Ocean sediments

Samuel D. Katz
*University of Rhode Island*

Roger Patrick Kelly
*University of Rhode Island*

Rebecca S. Robinson
*University of Rhode Island*, rebecca_r@uri.edu

Frank J. Pavia
*University of Rhode Island*

Robert Pockalny
*University of Rhode Island*, rpockalny@uri.edu

*See next page for additional authors*



## Citation/Publisher Attribution

Katz, S.D., Kelly, R.P., Robinson, R.S. *et al.* Biomass burning is a source of modern black carbon to equatorial Atlantic Ocean sediments. *Commun Earth Environ* 5, 536 (2024). https://doi.org/10.1038/s43247-024-01642-x
Available at: https://doi.org/10.1038/s43247-024-01642-x

# Biomass burning is a source of modern black carbon to equatorial Atlantic Ocean sediments




## Authors

Samuel D. Katz, Roger Patrick Kelly, Rebecca S. Robinson, Frank J. Pavia, Robert Pockalny, and Rainer Lohmann

communications earth & environment

Article

https://doi.org/10.1038/s43247-024-01642-x

# Biomass burning is a source of modern black carbon to equatorial Atlantic Ocean sediments



Samuel D. Katz [1] ✉, Roger Patrick Kelly [1], Rebecca S. Robinson [1], Frank J. Pavia [2], Robert Pockalny [1] & Rainer Lohmann [1]

Black carbon is a refractory form of organic carbon formed from the incomplete combustion of fossil fuels and biomass. Riverine transport is considered the dominant pathway of black carbon to the coastal oceans. However, the provenance and pathways of black carbon to the open ocean remain unknown. Here we use both stable and radiogenic isotopes of carbon to show that sedimentary black carbon across the equatorial Atlantic Ocean is aeolian and primarily derived from biomass burning of C4-plants. Fluxes of surface sedimentary black carbon measured along an equatorial Atlantic Ocean transect using chemothermal oxidation at 375 °C were relatively consistent across the Atlantic, ranging from 0.10–0.35 mg $cm^{-2}$ $kyr^{-1}$. Carbon isotope values near Africa suggest the black carbon was mostly young and derived from C4 plants, whereas offshore South America, the black carbon was older and dominated by C3 plants. The black carbon radiocarbon values were similar to the reservoir corrected total organic carbon near Africa, implying little pre-aging on land and increased westwards. These findings highlight the influence of C4-biomass burning in the tropical Atlantic and the importance of aeolian deposition as a black carbon source within the global carbon cycle.

Incomplete combustion from biomass burning and fossil fuels produces residual chars and fine particulates, commonly referred to as black carbon (BC)[1]. Globally, fossil fuels annually account for 5–13 Tg of BC emissions[2], while biomass burning produces 128 ± 84 Tg of BC annually[3], 2–11 Tg of which are released as BC aerosols (henceforth for refer to as soot BC) that are capable of long-range transport[4]. Soot BC is comprised of re-condensed volatile aromatic structures from burning, has low reactivity, and is thermally and chemically resistant[5,6], making it a refractory form of organic carbon (OC)[7]. BC originating from biomass burning transfers carbon from the fast-cycling biological carbon pool to the slower-cycling geological carbon pool, possibly leading to an overestimation of carbon dioxide release by wildfires[1,7–9]. Burial of this refractory soot BC is missing in the carbon budgets of global climate change models. One step towards resolving this issue is to increase our knowledge of sedimentary BC storage globally[7].

Globally, riverine fluxes of particulate BC to the oceans are an order of magnitude greater (17–37 Tg $yr^{-1}$)[3,10] than BC aerosol fluxes (2–5 Tg $yr^{-1}$)[10]. Fluvial particulate BC, similar to particulate OC, is believed to primarily be deposited on the continental margin[11,12]. Furthermore, although not well constrained, it is predicted that a majority of oceanic BC deposition (both aeolian and fluvial) occurs on the continental margins due to the proximity to terrestrial sources[7,10]. However, constraining BC cycling, residence time, and export to sediments in continental margin sediments present two challenges. First, riverine BC has been shown to be stored within the watershed before being transported to ocean sediments[11,13]. Secondly, inputs from the burning of fossil fuels, which are radiocarbon dead, presents a challenge when constraining the BC's age directly. Sedimentary BC from highly industrialized regions is strongly influenced by fossil fuel emissions[14]. These two factors lead to on-shelf sedimentary BC with older radiocarbon ages than the sedimentary total organic carbon in the Gulf of Maine[15], US east coast[14], Oregon coast[16], and deep ocean (pelagic) sedimentary BC from the Artic and[17], Pacific Oceans[16,18,19]. On the contrary, a recent study reported sedimentary BC at the Sierra Leone Rise to be modern and originated from African biomass burning[20].

Global satellite observations indicate that sub-Saharan Africa is a hot spot for large-scale biomass burning annually, including savannah and tropical slash and burn fires[1], accounting for >50% of the global carbonaceous aerosol budget[21,22]. Significant biomass burning occurs annually as a result of pan-African burning of crop fields[23] and dry-season fires, predominately from anthropogenic sources but also lightning strikes, that burn ~40% of northern African savannah grasses (December to March)[24]. Stable carbon isotope values can distinguish between plant types (e.g., grasses and sedges versus trees), allowing for estimates of their relative contributions to

[1]Graduate School of Oceanography, University of Rhode Island, Narragansett, RI, USA. [2]School of Oceanography, University of Washington, Seattle, WA, USA. ✉e-mail: sdkatz@uri.edu

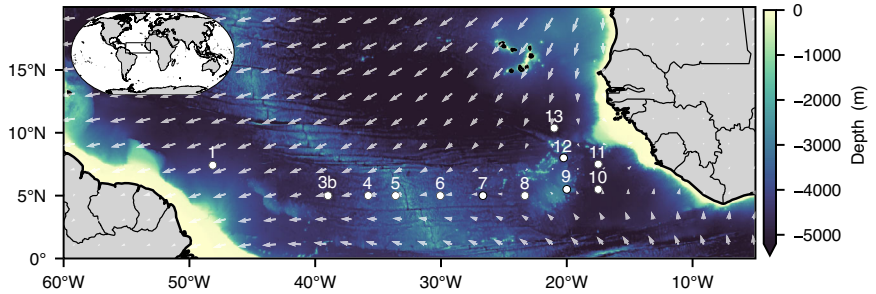


**Fig. 1 | Sediment samples sites with the depth and average yearly wind.** Sample sites from EN 651 with successful multicore samples recovered (white circles and labeled). Depth of the Equatorial Atlantic Ocean (colored background) (https://www.gebco.net). Surface level averaged yearly wind patterns from ECMWF Reanalysis v5 (white arrows) (https://www.ecmwf.int/en/forecasts/dataset/ecmwf-reanalysis-v5).

the sedimentary carbon pool. Sub-Saharan Africa has a mix of these plant types with C4 plants (i.e., grasses, with average $\delta^{13}C$ values of ~−15‰) dominant in northern regions, transitioning to C3 plants (i.e., trees, with a $\delta^{13}C$ of ~−26‰) dominant around the equator[25,26], resulting in a mixed $\delta^{13}C$ signature of carbonaceous aerosols (−17 to −15‰)[27] that is weighted towards the grasses of sub-Saharan Africa. Aerosols from the African continent are carried over the ocean by the trade winds, where they converge along the intertropical convergence zone (ITCZ) and are scavenged from the atmosphere by rainfall[28–30]. The residence time of BC aerosols is, on average, ~7 days in the equatorial Atlantic[31], leading to a large biomass-derived BC plume being transported offshore along the ITCZ[27], with smoke and phosphorus detected as far west as the Amazon Rain forest[32,33].

Given the transatlantic transport of African-derived biomass aerosols and the modern age of sedimentary BC found at the Sierra Leone Rise, here we assess the relative amount and source contributions of BC to pelagic and Amazon River influenced sediments in the equatorial Atlantic. To do so, we measured concentrations (using chemothermal oxidation at 375 °C (CTO 375)), fluxes (using extraterrestrial $^3He$ ($^3He_{ET}$)), sources (using $^{13}C$), and ages (using $^{14}C$) at 12 surface sediment sites across three distinct geographical regions of the equatorial Atlantic Ocean (the Sierra Leone Rise, Mid Atlantic region, and the Amazon River outflow) (Fig. 1). We note that the CTO 375 method isolates soot-like BC[34–36], the form most likely transported long distances from combustion sources[7,10]. $^3He_{ET}$ is a valuable measurement for aeolian-derived flux calculations, as it represents purely vertical deposition negating any post deposition sediment transport that could occur[37,38].

## Spatial distribution of black carbon

The concentration of surface pelagic sedimentary BC across the equatorial Atlantic ranges from 0.240 ± 0.029 mg $g^{-1}$ (site 8) to 0.614 ± 0.107 mg $g^{-1}$ (site 6) (Fig. 2), with no relation to distance from Africa ($r^2 = 0.14$) or precipitation ($r^2 = 0.07$) (SI Table 1). The lack of correlation with both distance and precipitation suggests there is lateral transport of BC as the particles sink through the water column, as precipitation is the main deposition pathway for aerosols[29]. A slight latitudinal increase was observed amongst the easternmost sites (closest to Africa), from 0.502 to 0.717 mg $g^{-1}$ over 550 km (Table 1), possibly due to the greater influence of the ITCZ removing BC particles over the northernmost site. Interestingly, our concentrations are an order of magnitude lower than previously reported for the Sierra Leone Rise (6.5 ± 3.1 mg $g^{-1}$)[20]. However, our concentrations are similar to continental shelf concentrations off the southern Atlantic USA (0.3–0.8 mg $g^{-1}$)[14] and the Gulf of Maine (0.3–1.7 mg $g^{-1}$)[39], and approximately half the off-shelf concentrations found off South America (1.1 ± 0.3 and ~1 mg $g^{-1}$)[20,30] and west of Portugal (1.26 mg $g^{-1}$)[40]. Comparisons to other studies, beyond what is presented above, are limited due to the differences between BC methodologies isolating different parts of the BC spectrum[7,35].

The relative contribution of BC to the sedimentary total organic carbon (TOC) pool (as % of TOC) in the equatorial Atlantic ranges from 4.2 to 13%, similar to or lower than previous observations, including shelf sediments from the Guinean Gulf (3–13%) and organic C poor sediments off northern Brazil (16–33%)[30].

$^3He_{ET}$ derived mass accumulation rates (MAR) range between 0.19 ± 0.08 and 0.64 ± 0.26 g $cm^{-2}$ $kyr^{-1}$ (Table 1) across the Atlantic basin. Resulting BC export fluxes range from 0.10 ± 0.04 mg $cm^{-2}$ $kyr^{-1}$ in the east (sites 8 and 10) to 0.36 ± 0.16 mg $cm^{-2}$ $kyr^{-1}$ in the central basin (site 6). The exception is site 1, on the Amazon River submarine fan off the shelf, with a BC flux of 1.14 ± 0.49 mg $cm^{-2}$ $kyr^{-1}$ (Fig. 2), which is likely impacted by additional fluvial BC fluxes.

## Isotopic shifts of black carbon

The eastward increase in $\delta^{13}C_{BC}$ values from −20.9‰ (site 4) to −17.4‰ (site 10) and in $\Delta^{14}C_{BC}$ values from −412‰ (site 3b) to −172‰ (site 10) across the equatorial Atlantic transect (Fig. 2) suggests BC sources varied in both their relative contributions of C3 and C4 plants and biomass vs. fossil fuel sourced BC.

On the eastern side of the Atlantic basin, the $\Delta^{14}C$ BC values are essentially the same as the reservoir corrected $\Delta^{14}C$ TOC values ($\Delta\Delta^{14}C$ 18‰) (Fig. 3) at site 10. This is the third reported instance of coeval BC found in marine sediments[14], and the second in pelagic sediments[20]. Furthermore, at site 13, BC and TOC again essentially have the same $\Delta^{14}C$ values with a $\Delta\Delta^{14}C$ of −58‰. Given the depletion in $\delta^{13}C_{BC}$, we assume that the difference between $\Delta^{14}C$ of site 10 and 13 is caused by increased fossil fuel emissions from Europe and Africa carried along the northeast trade winds[28]. These findings challenge the previous assumption that oceanic sedimentary BC is primarily pre-aged and delivered fluvially[11,41], suggesting that a more regional approach to examining sedimentary BC is needed to determining BC sources on a global scale.

To assess the relative importance of biomass and fossil fuel emission sources, we use a progressive two-step, two-isotope mixing model, where we first determine the fossil fuel contribution to remove that fraction to obtain the $\delta^{13}C$ value of biomass burning and fraction of C3 plants. In essence, fossil fuel emissions contribute between 28 and 29% to BC in the western Atlantic Basin (sites 3b & 5) and between 0 and 25% in the eastern Atlantic Basin (sites 7 & 10). We note that fossil fuel emissions probably contribute somewhat to the $\Delta^{14}C$ value at site 10; however, we are unable to determine the exact fraction because BC and TOC have the effectively same $\Delta^{14}C$ values. Note that the isotopic mixing model used here is highly dependent on the $\delta^{13}C$ values used in this analysis. We used a two-isotope mixing model due to the physical isolation and the recalcitrant nature of the fine soot BC analyzed in this study.

The contribution of C3 plants (trees) (Eq. 3) is between 32% and 48% in the western Atlantic Basin and between 10% and 24% in the eastern Atlantic Basin (Table 2). These shifts between the eastern and western samples are indicative of changing source(s). In the eastern Atlantic Basin, northern sub-Saharan grassland burns, dominant during the Austral summer, produce BC which is transported by the trade winds to the ITCZ and deposited[28,31]. Towards the western basin, southern African grassland and Congo rainforest burn emissions, dominant during the Austral winter, are transported further across the Atlantic by the trade winds with the northern movement of the ITCZ[32].

A recent study examining the fraction of atmospheric particulate elemental carbon (EC), which is similar to the BC detected via the CTO-375

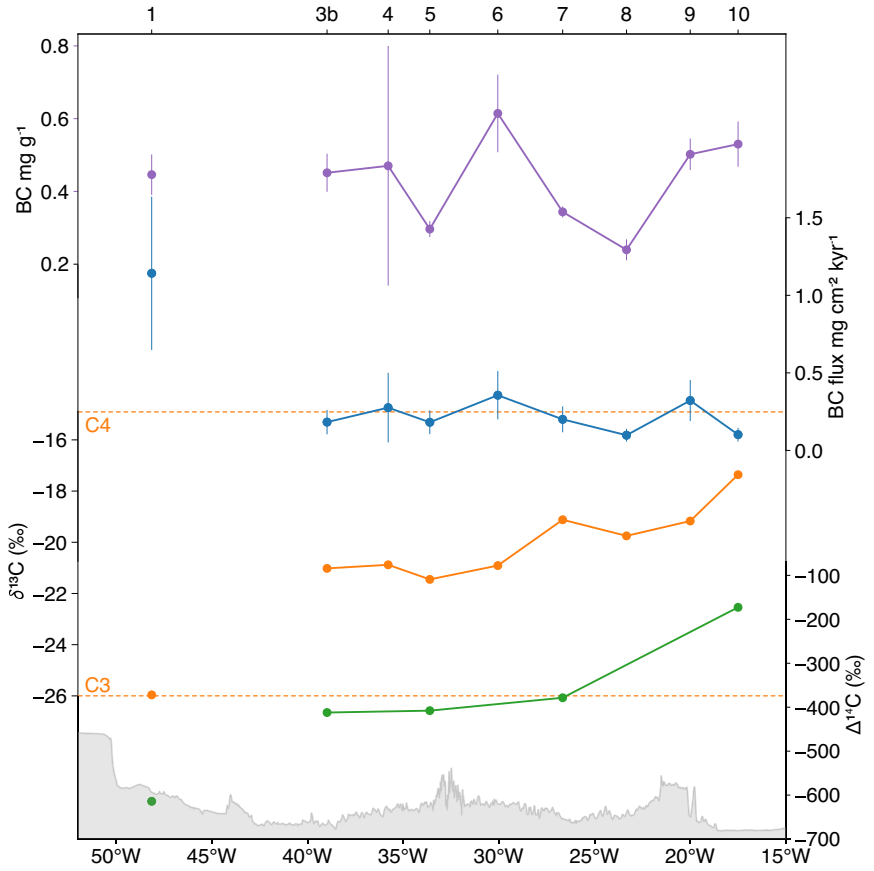


**Fig. 2 | Concentration, flux, $\delta^{13}C_{BC}$, $\Delta^{14}C_{BC}$ from Atlantic transect at ~5°N.** The concentrations (mg $g^{-1}$; purple), flux (mg $cm^{-2}$ $kyr^{-1}$; blue), $\delta^{13}C$ (‰; orange), and $\delta^{14}C$ (‰; green) from this transect with bathymetry (bottom gray) illustrating the bathymetric changes across the Equatorial Atlantic Ocean. Values from the site 1 (the Amazon River outflow) are not considered part of the 5°N transect and originate from a different source, further illustrating the differences between aeolian and riverine BC sources.

**Table 1 | Concentration, fluxes, isotopic measurements from Equatorial Atlantic Ocean**

| Site | MAR (g $cm^{-2}$ $kyr^{-1}$ (n)) | TOC (mg $g^{-1}$) | TOC $\delta^{13}C$ (‰) | TOC $\Delta^{14}C$ (‰) | BC (mg $g^{-1}$) | BC flux (mg $cm^{-2}$ $kyr^{-1}$) | BC $\delta^{13}C$ (‰) | BC $\Delta^{14}C$ (‰) | $f_{FF}$ |
|---|---|---|---|---|---|---|---|---|---|
| 1 | 2.56 ± 1.06 (2) | 6.72 | −21.37 | −292.56 | 0.446 ± 0.055 | 1.09 ± 0.49 | −25.96 | −614.09 | |
| 3b | 0.4 ± 0.17 (2) | 9.66 | −20.05 | −212.85 | 0.451 ± 0.052 | 0.18 ± 0.08 | −21.02 | −412.06 | 29% |
| 4 | 0.59 ± 0.24 (2) | 5.07 | −18.58 | | 0.470 ± 0.329 | 0.27 ± 0.22 | −20.88 | | |
| 5 | 0.61 ± 0.25 (2) | 4.87 | −18.73 | −194.55 | 0.296 ± 0.022 | 0.18 ± 0.08 | −21.45 | −407.81 | 28% |
| 6 | 0.58 ± 0.23 (3) | 4.67 | −18.46 | | 0.614 ± 0.107 | 0.35 ± 0.16 | −20.91 | | |
| 7 | 0.58 ± 0.24 (2) | 5.74 | −17.11 | −187.48 | 0.344 ± 0.015 | 0.2 ± 0.08 | −19.12 | −378.45 | 25% |
| 8 | 0.41 ± 0.16 (3) | 5.64 | −19.65 | | 0.240 ± 0.029 | 0.1 ± 0.04 | −19.75 | | |
| 9 | 0.64 ± 0.26 (3) | 7.46 | −18.30 | | 0.502 ± 0.043 | 0.32 ± 0.13 | −19.17 | | |
| 10 | 0.19 ± 0.08 (2) | 10.13 | −18.44 | −244.3 | 0.530 ± 0.062 | 0.1 ± 0.04 | −17.36 | −172.67 | 0 |
| 11 | | 10.22 | −18.65 | | 0.645 ± 0.002 | | −19.14 | | |
| 12 | 0.51 ± 0.21 (2) | 6.12 | −18.39 | | 0.534 ± 0.112 | 0.27 ± 0.13 | −19.52 | | |
| 13 | 0.49 ± 0.2 (2) | 9.37 | −18.22 | −266.29 | 0.717 ± 0.059 | 0.34 ± 0.15 | −20.13 | −272.38 | 12% |

Mass Accumulation rates (MARs) measured in duplicate or triplicate (indicated in table) error on the MARs account for both the uncertainty on $^3He_{ET}$ and in the extraterrestrial $^3He$ flux. The BC concentrations were measured in triplicates and the reported error is the standard deviation of the three samples. BC fluxes were derived from the MARs and BC concentration values with propagation of error values.

method[7,27], found that the $\delta^{13}C$ of savanna EC is further depleted during combustion, by −2.4 ± 1.9‰ in laboratory experiments and −6.8 ± 1.1‰ in natural fires[42]. Another study showed that the $\delta^{13}C$ of char remains of C3 plants are enriched by ~1‰. To date, there are no studies examining the fractionation of $\delta^{13}C$ during combustion utilizing the CTO-375 method. To reflect these potential changes to $\delta^{13}C$ post-emission, we evaluated four scenarios; (i) no change in $\delta^{13}C$ stable isotope ratios post burn; (ii) stable isotope fractionations with a $\delta^{13}C$ endmember of both −26‰ and −25‰ values for C3 plants; (iii) −15‰ and −16‰ values for C4 plants; and (iv) both C3 and C4 endmembers changed (Table 2). Changes to the $\delta^{13}C_{C4}$ endmember reflect a greater change in our mixing model as a greater proportion of the BC at our sites are from C4 plants.

BC isotopes from the Amazon River outflow (site 1) display carbon isotope signatures that are distinctly different from the mid-Equatorial Atlantic sampling locations, indicating that the pelagic Atlantic locations are isolated from the Amazon's influence (Fig. 2). The $\Delta^{14}C_{BC}$ value of riverine particulate black carbon from the Amazon was previously reported to range between −333‰ to −439‰ $\Delta^{14}C_{BC}$[11], higher than our marine sediment at −614‰ $\Delta^{14}C_{BC}$, probably a reflection of differing depositional histories between the river derived shelf and pelagic sediments. These differences may

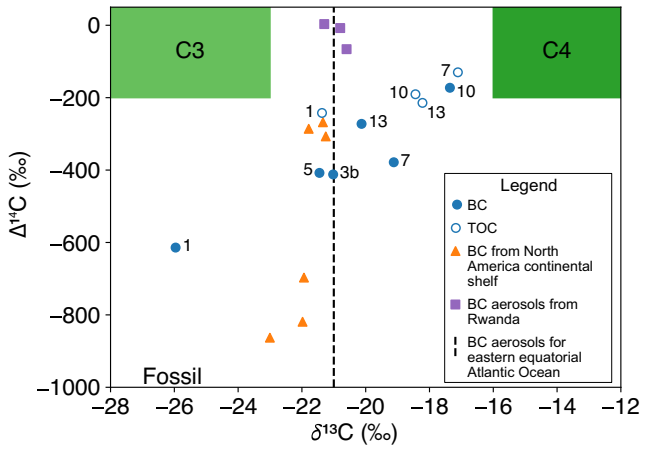


**Fig. 3 | Carbon isotopic comparison of source and age.** The biomass endmembers are labeled in green boxes and fossil fuel endmember along the bottom. BC aerosols from the Rwanda Climate Observatory (purple squares)[21] and Equatorial Atlantic Ocean (vertical dashed line, as age was not measured)[27] represent the African biomass burning aerosol plume. The results from our sedimentary BC (solid blue circles) and TOC (hollow blue circles) are labeled with the samples sites. Sedimentary BC from the North America continental shelf (orange triangles)[14] represent the only other Atlantic sedimentary BC values.

**Table 2 | Stable isotope mixing model shifts with potential fractionation during biomass burning**

| Site | $\delta^{13}C_{BB}$ | $F_{C3}$ with | | | |
|---|---|---|---|---|---|
| | | Original values | Enriched C3 | Depleted C4 | Both enriched C3 and depleted C4 |
| 3b | −19.2 | 38% | 42% | 32% | 36% |
| 5 | −19.8 | 44% | 48% | 38% | 43% |
| 7 | −17.0 | 18% | 20% | 10% | 11% |
| 10 | −17.4 | 21% | 24% | 14% | 15% |
| 13 | −19.4 | 40% | 44% | 34% | 38% |

Shown are the $\delta^{13}C_{BB}$ mixing model results with our stated end members C3 plants (−26‰) and C4 plants (−15‰). Included are 3 scenarios showing deviations from the original mixing model, reflecting potential $\delta^{13}C$ fractionations that could occur during biomass burning (i) The enriched C3-$\delta^{13}C$ increases to −25‰ reflecting the potential for woody substances to be enriched up to 1‰ postburn[53]; (ii) The depleted C4-$\delta^{13}C$ decreases to −16‰, reflecting that the $\delta^{13}C$ in BC aerosols have been detected to decrease by −1‰ to −6‰ depending on the biome[42]; (iii) both changes were included to calculate the mixing model.

in part also be due to methodical differences, where the riverine particles were oxidized condensed polyaromatic moieties to benzenepolycarboxylic acids (BPCAs)[43], while we used thermal oxidation of the OC before radiocarbon measurement of the BC[35].

## Implications for the global black carbon cycle

Our findings of young, pelagic, aeolian-transported BC originating primarily from African biomass burning highlights regional differences of BC fate and transport. Fluxes of BC on the Atlantic continental shelf, at 87–250 μg $cm^2$ $yr^{-1}$ [14], are 2 to 3 orders of magnitude greater than the fluxes presented here. Yet despite the decreased sedimentation rate, sediment close to Africa (site 10 and 13) have $\Delta^{14}C$ of −173‰ and −272‰, slightly enriched and similar to sedimentary BC $\Delta^{14}C$ values reported for the Florida Strait, of −286‰ and −268‰, at depths corresponding to 2017 and 1989, respectively[14]. These findings suggest that BC is settling out of the water column quickly. BC fluxes in the remote pelagic Pacific Ocean at 0.048 mg $cm^{-2}$ $kyr^{-1}$, are similar to our deep ocean Atlantic fluxes. Yet, the $\Delta^{14}C$ value of sedimentary BC, −731‰ $\Delta^{14}C$, is significantly more depleted than our most depleted pelagic sediment, −412‰ $\Delta^{14}C$[16]. This highlights the differences in both source and transportation pathways between the equatorial Atlantic and equatorial Pacific BC. At another site in the deep Pacific Ocean along the California current, the $\Delta^{14}C$ value of surface sedimentary BC ranged between −530 ± 7‰ and −740 ± 36‰ $\Delta^{14}C_{BC}$, similar to our sample from the Amazon river outflow (−614‰ $\Delta^{14}C$), regardless of slight variations from the differing methods utilizing BPCAs[19,35]. These results from the Atlantic and Pacific further highlight the significance of finding young BC in pelagic sediments across the entire tropical Atlantic Ocean, which has been quickly exported from the fast cycling biological carbon pool to the slower geological carbon pool.

The geographical and study associated differences highlight major challenges to be addressed in future work[7]: (1) More pelagic BC measurements that include radiocarbon values of BC are needed to better constrain BC export to sediments. (2) A regional approach is needed to examine BC export to pelagic sediments. As we demonstrated for the tropical Atlantic Ocean, aeolian deposition can be important regionally. Any approach to examining BC export should encompass regional systems rather than only point source contributions (i.e., riverine transport). (3) A lack of inter-laboratory and inter-method comparisons limits our understanding of BC sources and fluxes between studies and regions. Currently, there are three approaches regularly employed to quantify BC in sediments (i) the CTO 375[14,30,39], (ii) BPCAs[11,19,44], and (iii) thermal/optical transmittance and reflectance[41], all which isolate a different fraction of BC and thus produce different results for the limited standard reference materials (SRMs) available[35]. Further work is needed to both create new SRMs and conduct a methodological comparison with both SRMs and environmental samples.

Here we present new findings on the fluxes, providence, and age of sedimentary BC in the Equatorial Atlantic Ocean. We report on the regional abundance of radiocarbon-young BC from C4 plants originating from the northern sub-Saharan Africa. The back trajectories of several aerosol studies in the region[27–29,32] implies aeolian transport as the dominant pathway. Closest to Africa, the radiocarbon BC age is more modern than the sedimentary organic carbon fraction, but decreases westward across the Atlantic, as do the fraction of C4 plants. A major change in radiocarbon and C3 isotope ratios is evident close to the South American coast of the tropical Atlantic Ocean, impacted by the influence of the Amazon River. These results emphasize the need to consider the competing impacts of riverine versus aeolian emission plumes, and biomass versus fossil fuel emissions, on BC signatures and sedimentary fluxes.

## Methods

### Sample collection

We collected sediment samples using a MC-800 multicorer from 12 sites in the Equatorial Atlantic Ocean along a transect at 5°N aboard the *R.V. Endeavor* during the EN651 cruise from February to March 2020 (SI Table 1). All multicores were between 23 and 48 cm in depth, one core from each of the sites was sectioned on board at 1 cm intervals for the first 10 cm then 2 cm up to 20 cm depth. The sectioned cores were placed in amber glass jars and stored at −20 °C.

### Black carbon quantification and isotopic analysis

Surface sediment samples (0–1 cm) were dried at 60 °C and passed through a 420 μm sieve before analysis. TOC samples were weighed into silver capsules (Elemental microanalysis silver capsules ultra-clean pressed 8 × 5 mm, D2030), acidified to remove inorganic carbon (2 M HCl), and folded into tin capsules (Costech tin capsules 10 × 10 mm, 041073). BC was isolated using the CTO 375 method[34]. 100 mg of samples where weighed out into ceramic crucibles and spread into a thin layer to prevent charring. Samples were combusted at 375 °C for 24 h. under the flow of ultra high purity air (0.4 L $min^{-1}$). The remaining sediment was transferred to GC vials for storage, then processed the same as the TOC samples to remove any inorganic carbon present (as detailed above). Quantification of BC and TOC samples was performed using an Elemental Analyzer (Costech 4010

Elemental Analyzer). The stable carbon isotopes were measured using the elemental analyzer coupled to an Isotope Ratio Mass Spectrometer (Thermo Delta V Advantage). Radiocarbon isotopes were measured at the National Ocean Sciences Accelerator Mass spectrometry (NOSAMS).

Our $\delta^{13}C$ values with the influence of fossil fuels removed were calculated based on two assumptions. First, all sites other than from the Amazon River outflow (site 1) are sourced exclusively through aeolian deposition, as fluvial transport of particulate BC should mimic that of particulate OC[11,12]. Second, the difference in age between the sites is due to additional fossil fuels contributions, given that the only likely source is from aeolian biomass burning particles that are modern[21]. These calculations were performed in 3 steps to determine the $\delta^{13}C$ of biomass burning. We determined the fraction of the samples that is derived from fossil fuel emissions:

$$f_{FF} = \frac{\Delta^{14}C_{sample} - \Delta^{14}C_m}{\Delta^{14}C_{FF} - \Delta^{14}C_m} \quad (1)$$

Where $f_{FF}$ is the fraction fossil fuels,

$\Delta^{14}C_{sample}$ is the $\Delta^{14}C$ of our sample,

$\Delta^{14}C_m$ is the sediment from site 10 (−17.36‰, the youngest BC in sediment), and

$\Delta^{14}C_{FF}$ is radiocarbon dead (−1000‰).

We use this to determine the $\delta^{13}C$ from biomass burning was derived by removing the fossil fuel influence:

$$\delta^{13}C_{BB} = \frac{\delta^{13}C_{sample} - \delta^{13}C_{FF} \cdot f_{FF}}{(1 - f_{FF})} \quad (2)$$

where $\delta^{13}C_{BB}$ is the $\delta^{13}C$ of biomass burning,

$\delta^{13}C_{sample}$ is the $\delta^{13}C$ of our sample,

$\delta^{13}C_{FF}$ is the $\delta^{13}C$ of fossil fuel (−25.5‰)[45],

$\delta^{13}C_{C4}$ is the $\delta^{13}C$ of C4 plants (−15‰), and

$\delta^{13}C_{C3}$ is the $\delta^{13}C$ of C3 plants (−26‰)[25].

We then again used a two-isotope mixing model to derive the relative C3 plant contributions:

$$f_{C3} = \frac{\delta^{13}C_{BB} - \delta^{13}C_{C4}}{(\delta^{13}C_{C3} - \delta^{13}C_{C4})} \quad (3)$$

Radiocarbon TOC values were calibrated using a reservoir age of 550 years[46]. Due to the limited understanding of black carbon formation and the possibility of fossil fuel influence, the BC $\Delta^{14}C$ values were not calibrated.

### QA/QC

We measured all BC concentrations in triplicates, reporting the mean and standard deviation. Blank samples of pre-combusted sand were included with every oxidation and any positive carbon values were subtracted from the samples. A standard reference material (SRM 1941b marine sediment) was also included with every oxidation averaging 5.6 ± 0.3 mg $g^{-1}$ ($n = 5$), in line with previously reported concentrations of 5.8 ± 0.5 mg $g^{-1}$ [47], 5.7 ± 0.28 mg $g^{-1}$ [36], 5.3 ± 1.4 mg $g^{-1}$ [30], 6.1 ± 0.63 mg $g^{-1}$ [14].

### Helium isotope analyses

Helium isotopes were measured at the Farley Lab at Caltech, following previously published procedures[48,49]. Briefly, freeze-dried sample powders were leached to remove calcium carbonate in 10% acetic acid overnight. The residue was rinsed twice with deionized water and dried overnight at 60 °C. Then, 50–100 mg of decarbonated sample residue was packed into tin foil balls, loaded into an ultrahigh vacuum autosampler for introduction to a vacuum furnace. Before sample analysis, the furnace was outgassed at >1300 °C. Each sample was fused at 1200 °C in the vacuum furnace, with evolved gas purified by a charcoal-bearing U-trap at liquid nitrogen temperatures, followed by exposure to three SAES NP10 getters. The remaining gases were cryo-focused at 14 K, released at 34 K and measured on a Thermo Helix SFT mass spectrometer. Typical relative uncertainties on $^3He$ and $^4He$ concentrations were 1–2%.

### Mass accumulation rate determinations using $^3He_{ET}$

Computing mass accumulation rates from helium isotope measurements requires isolating the extraterrestrial component of the total $^3He$, which has both terrestrial and extraterrestrial sources. We calculate $^3He_{ET}$ using via two endmember mixing between terrestrial helium ($^3He/^4He = 2.0 \times 10^{-8}$)[50] and extraterrestrial helium ($^3He/^4He = 2.4 \times 10^{-4}$)[51]:

$$^3He_{ET} = \left( \frac{1 - \frac{\left[^3He/^4He\right]_{Terr}}{\left[^3He/^4He\right]_{Meas}}}{1 - \frac{\left[^3He/^4He\right]_{Terr}}{\left[^3He/^4He\right]_{IDP}}} \right) * {}^3He_{Meas} \quad (4)$$

Here, the subscripts "Terr", "IDP" and "Meas" refer to terrestrial, extraterrestrial, and measured, respectively. We compute mass accumulation rates by dividing the measured $^3He_{ET}$ concentrations by the extraterrestrial $^3He$ flux, which is constant in space and time during the late Quaternary at $f_{3He} = 0.8 \pm 0.3$ pcc STP $^3He_{ET}/cm^2/kyr$[51]:

$$MAR = \frac{f_{3He,ET}}{^3He_{ET,meas}} \quad (5)$$

Uncertainties arise in $^3He_{ET}$ due to heterogenous sampling of discrete interplanetary dust particles bearing $^3He$ in sediments[52]. Thus, reproducibility of duplicate measurements of $^3He$ exceeds analytical uncertainty. We measured all samples in duplicate, and some in triplicate. We followed previous approaches[37] in using the median fractional difference between duplicate samples as the basis for uncertainty on $^3He_{ET}$ concentrations, and thus on MARs. The median fractional difference in our study is 25%. We divide this median fractional difference by √n, where n is the number of duplicate samples run (either 2 or 3 in this study). Reported errors on MARs take into account both uncertainty on $^3He_{ET}$ and in the extraterrestrial $^3He$ flux.

### Precipitation and wind calculations

Monthly global data from 1940 to 2023 was obtained from European Centre for Medium-Range Weather Forecasts (ECMWF) Reanalysis version 5 consisting of U and V components of the 10 m wind and total precipitation and the temporarily data was removed. For the wind, the model output was coarsened to a 2° grid to improve computational performance and the U and V components were averaged monthly over the 80-year period. The precipitation was calculated on the 0.25° downloaded resolution taking the average again over monthly the 80-year period.

### Distance from Africa calculations

Preliminary analysis of sites' distance from Africa was measured using GeoMapApp by clicking and dragging to find the closest point on the coast, values were rounded to the nearest 10 km. This preliminary analysis showed no correlation with distance from Africa, so it was not pursued further.

### Reporting summary

Further information on research design is available in the Nature Portfolio Reporting Summary linked to this article.

## Data availability

Data generated as part of this work is publicly available on Zenodo (https://doi.org/10.5281/zenodo.12802502) and via the Biological & Chemical Ocean Data Management Office (BCO-DMO) project number 818636.

Received: 6 November 2023; Accepted: 22 August 2024;
Published online: 30 September 2024

## References


1. Jones, M. W., Santín, C., van der Werf, G. R. & Doerr, S. H. Global fire emissions buffered by the production of pyrogenic carbon. *Nat. Geosci.* **12**, 742–747 (2019).
2. Bond, T. C. et al. Bounding the role of black carbon in the climate system: a scientific assessment. *J. Geophys. Res. Atmospheres* **118**, 5380–5552 (2013).
3. Jones, M. W. et al. Fires prime terrestrial organic carbon for riverine export to the global oceans. *Nat. Commun.* **11**, 2791 (2020).
4. Santín, C. et al. Towards a global assessment of pyrogenic carbon from vegetation fires. *Glob. Change Biol.* **22**, 76–91 (2016).
5. Schmidt, M. W. I. & Noack, A. G. Black carbon in soils and sediments: analysis, distribution, implications, and current challenges. *Glob. Biogeochem. Cycles* **14**, 777–793 (2000).
6. Masiello, C. A. New directions in black carbon organic geochemistry. *Mar. Chem.* **92**, 201–213 (2004).
7. Coppola, A. I. et al. The black carbon cycle and its role in the Earth system. *Nat. Rev. Earth Environ.* **3**, 516–532 (2022).
8. Harrison, S. P. et al. The biomass burning contribution to climate–carbon-cycle feedback. *Earth Syst. Dyn.* **9**, 663–677 (2018).
9. Bowring, S. P. K., Jones, M. W., Ciais, P., Guenet, B. & Abiven, S. Pyrogenic carbon decomposition critical to resolving fire's role in the Earth system. *Nat. Geosci.* **15**, 135–142 (2022).
10. Bird, M. I., Wynn, J. G., Saiz, G., Wurster, C. M. & McBeath, A. The pyrogenic carbon cycle. *Annu. Rev. Earth Planet. Sci.* **43**, 273–298 (2015).
11. Coppola, A. I. et al. Global-scale evidence for the refractory nature of riverine black carbon. *Nat. Geosci.* **11**, 584–588 (2018).
12. Hedges, J. I. & Keil, R. G. Sedimentary organic matter preservation: an assessment and speculative synthesis. *Mar. Chem.* **49**, 81–115 (1995).
13. Hanke, U. M. et al. What on Earth have we been burning? Deciphering sedimentary records of pyrogenic carbon. *Environ. Sci. Technol.* **51**, 12972–12980 (2017).
14. Wulandari, I., Katz, S., Kelly, R. P., Robinson, R. S. & Lohmann, R. Sedimentary accumulation of black carbon on the east coast of The United States. *Geophys. Res. Lett.* **50**, e2022GL101509 (2023).
15. Flores-Cervantes, D. X., Plata, D. L., MacFarlane, J. K., Reddy, C. M. & Gschwend, P. M. Black carbon in marine particulate organic carbon: Inputs and cycling of highly recalcitrant organic carbon in the Gulf of Maine. *Mar. Chem.* **113**, 172–181 (2009).
16. Dickens, A. F., Gélinas, Y., Masiello, C. A., Wakeham, S. & Hedges, J. I. Reburial of fossil organic carbon in marine sediments. *Nature* **427**, 336–339 (2004).
17. Ren, P. et al. Sources and sink of black carbon in Arctic Ocean sediments. *Sci. Total Environ.* **689**, 912–920 (2019).
18. Masiello, C. A. & Druffel, E. R. M. Black carbon in deep-sea sediments. *Science* **280**, 1911–1913 (1998).
19. Coppola, A. I., Ziolkowski, L. A., Masiello, C. A. & Druffel, E. R. M. Aged black carbon in marine sediments and sinking particles. *Geophys. Res. Lett.* **41**, 2427–2433 (2014).
20. Laurent, K., Cantwell, M. & Lohmann, R. New insights on black carbon in pelagic Atlantic sediments. *Mar. Chem.* **257**, 104312 (2023). St.
21. Kirago, L. et al. Atmospheric black carbon loadings and sources over eastern sub-Saharan Africa are governed by the regional savanna fires. *Environ. Sci. Technol.* **56**, 15460–15469 (2022).
22. Ramo, R. et al. African burned area and fire carbon emissions are strongly impacted by small fires undetected by coarse resolution satellite data. *Proc. Natl. Acad. Sci. USA* **118**, e2011160118 (2021).
23. Curtis, P. G., Slay, C. M., Harris, N. L., Tyukavina, A. & Hansen, M. C. Classifying drivers of global forest loss. *Science* **361**, 1108–1111 (2018).
24. Cachier, H., Buat-Menard, P., Fontugne, M. & Rancher, J. Source terms and source strengths of the carbonaceous aerosol in the tropics. *J. Atmospheric Chem.* **3**, 469–489 (1985).
25. Holtvoeth, J., Wagner, T. & Schubert, C. J. Organic matter in river-influenced continental margin sediments: the land-ocean and climate linkage at the Late Quaternary Congo fan (ODP Site 1075). *Geochem. Geophys. Geosystems* **4**, 1–27 (2003).
26. Collins, J. A. et al. Interhemispheric symmetry of the tropical African rainbelt over the past 23,000 years. *Nat. Geosci.* **4**, 42–45 (2011).
27. Pohl, K., Cantwell, M., Herckes, P. & Lohmann, R. Black carbon concentrations and sources in the marine boundary layer of the tropical Atlantic Ocean using four methodologies. *Atmospheric Chem. Phys.* **14**, 7431–7443 (2014).
28. Eglinton, T. I. et al. Composition, age, and provenance of organic matter in NW African dust over the Atlantic Ocean. *Geochem. Geophys. Geosystems* **3**, 1–27 (2002).
29. Yu, H. et al. Estimates of African dust deposition along the trans-Atlantic transit using the decadelong record of aerosol measurements from CALIOP, MODIS, MISR, and IASI. *J. Geophys. Res. Atmospheres* **124**, 7975–7996 (2019).
30. Lohmann, R. et al. Fluxes of soot black carbon to South Atlantic sediments. *Glob. Biogeochem. Cycles* **23**, 1–13 (2009).
31. Reddy, M. S. & Boucher, O. Climate impact of black carbon emitted from energy consumption in the world's regions. *Geophys. Res. Lett.* **34**, 1–5 (2007).
32. Holanda, B. A. et al. African biomass burning affects aerosol cycling over the Amazon. *Commun. Earth Environ.* **4**, 1–15 (2023).
33. Barkley, A. E. et al. African biomass burning is a substantial source of phosphorus deposition to the Amazon, Tropical Atlantic Ocean, and Southern Ocean. *Proc. Natl. Acad. Sci. USA* **116**, 16216–16221 (2019).
34. Gustafsson, Ö. et al. Quantification of the dilute sedimentary soot phase: implications for PAH speciation and bioavailability. *Environ. Sci. Technol.* **31**, 203–209 (1997).
35. Hammes, K. et al. Comparison of quantification methods to measure fire-derived (black/elemental) carbon in soils and sediments using reference materials from soil, water, sediment and the atmosphere. *Glob. Biogeochem. Cycles* **21**, 1–18 (2007).
36. Elmquist, M., Cornelissen, G., Kukulska, Z. & Gustafsson, Ö. Distinct oxidative stabilities of char versus soot black carbon: implications for quantification and environmental recalcitrance. *Glob. Biogeochem. Cycles* **20**, 1–11 (2006).
37. Abell, J. T., Winckler, G., Anderson, R. F. & Herbert, T. D. Poleward and weakened westerlies during Pliocene warmth. *Nature* **589**, 70–75 (2021).
38. Farley, K. A., Maier-Reimer, E., Schlosser, P. & Broecker, W. S. Constraints on mantle 3He fluxes and deep-sea circulation from an oceanic general circulation model. *J. Geophys. Res. Solid Earth* **100**, 3829–3839 (1995).
39. Gustafsson, Ö. & Gschwend, P. M. The flux of black carbon to surface sediments on the New England continental shelf. *Geochim. Cosmochim. Acta* **62**, 465–472 (1998).
40. Middelburg, J. J., Nieuwenhuize, J. & van Breugel, P. Black carbon in marine sediments. *Mar. Chem.* **65**, 245–252 (1999).
41. Fang, Y. et al. Particulate and dissolved black carbon in coastal China Seas: spatiotemporal variations, dynamics, and potential implications. *Environ. Sci. Technol.* **55**, 788–796 (2021).
42. Vernooij, R. et al. Stable carbon isotopic composition of biomass burning emissions—implications for estimating the contribution of $C_3$ and $C_4$ plants. *Atmospheric Chem. Phys.* **22**, 2871–2890 (2022).
43. Dittmar, T. The molecular level determination of black carbon in marine dissolved organic matter. *Org. Geochem.* **39**, 396–407 (2008).
44. Coppola, A. I. & Druffel, E. R. M. Cycling of black carbon in the ocean. *Geophys. Res. Lett.* **43**, 4477–4482 (2016).

45. Widory, D. Combustibles, fuels and their combustion products: a view through carbon isotopes. *Combust. Theory Model.* **10**, 831–841 (2006).
46. Heaton, T. J. et al. Marine20—the marine radiocarbon age calibration curve (0–55,000 cal BP). *Radiocarbon* **62**, 779–820 (2020).
47. Gustafsson, Ö. et al. Evaluation of a protocol for the quantification of black carbon in sediments. *Glob. Biogeochem. Cycles* **15**, 881–890 (2001).
48. Mukhopadhyay, S., Farley, K. A. & Montanari, A. A Short Duration of the Cretaceous-Tertiary Boundary Event: Evidence from Extraterrestrial Helium-3. *Science*. **291**, 1952–1955 (2003).
49. Schmitz, B. et al. An extraterrestrial trigger for the mid-Ordovician ice age: Dust from the breakup of the L-chondrite parent body. *Sci. Adv.* **5**, 1–10 (2019).
50. Farley, K. A. Cenozoic variations in the flux of interplanetary dust recorded by3He in a deep-sea sediment. *Nature* **376**, 153–156 (1995).
51. McGee, D. & Mukhopadhyay, S. in *The Noble Gases as Geochemical Tracers* (ed. Burnard, P.) 155–176 (Springer, 2013).
52. Farley, K. A., Love, S. G. & Patterson, D. B. Atmospheric entry heating and helium retentivity of interplanetary dust particles. *Geochim. Cosmochim. Acta* **61**, 2309–2316 (1997).
53. Bostick, K. W. et al. Production and composition of pyrogenic dissolved organic matter from a logical series of laboratory-generated chars. *Front. Earth Sci.* **6**, 1–14 (2018).

## Acknowledgements

We acknowledge support from NSF OCE award #1924191 awarded to Rainer Lohmann. We thank Benjamin Gayman (Harvard University) for connecting URI authors with Frank Pavia to include his work on the $^{3}He_{ET}$ MARs, as well as Kenneth Farley and Jonathan Treffkorn (California Institute of Technology) for laboratory and instrument time for the $^{3}He_{ET}$ measurements. We would also like to acknowledge the crew and marine scientist of the *R.V. Endeavor* for their work in recovering deep ocean multicores, especially marine technician Gabe Matthias and MATE-at-Sea intern Lydia Sgouros.

## Author contributions

R.L. and R.P. served as co-PIs on the research grant. S.K. and R.L. led the sample collection, with R.P. assisting in site selection. S.K. performed most of the analyses and interpretation, while R.K. provided methodological and analytical assistance, and F.P. conducted the $^{3}He$ isotope analyses. R.R. assisted in the data interpretation. S.K. wrote the majority of the manuscript and all authors reviewed and edited the manuscript.

## Competing interests

The authors declare no competing interests.

## Additional information

**Supplementary information** The online version contains supplementary material available at https://doi.org/10.1038/s43247-024-01642-x.

**Correspondence** and requests for materials should be addressed to Samuel D. Katz.

**Peer review information** *Communications Earth & Environment* thanks the anonymous reviewers for their contribution to the peer review of this work. Primary Handling Editors: Sze Ling Ho, Clare Davis, Alice Drinkwater, and Martina Grecequet. A peer review file is available.